Structural Transitions in Polydiacetylene Langmuir Films

Yevgeniy Lifshitz, Yuval Golan, Oleg Konovalov and Amir Berman

Note:

This is an updated report, replacing the original SI-1016 report.

This report is based on a manuscript submitted to *Langmuir*.

Abstract

Polydiacetylene (PDA) Langmuir films (LF) were investigated directly at the air/water interface using *in-situ* synchrotron grazing incidence x-ray diffraction, and *ex-situ* using transmissison electron microscopy and diffraction. The films were deposited on pure water, without addition of metal cations or any other chemical substance. A crystallographic model describes the structures and phase transitions of the unpolymerized (monomer) film, via the metastable (blue phase), to the fully stable phase of PDA (red phase) as a function of irradiation. The monomer-to-blue-to-red chromatic phase transitions are accompanied by variations in crystal structure and molecular alignment within the LF. Notably, the characteristic linear strand morphology of these films is likely to result from the prominent decrease in (02) spacing upon transition from the blue to the red phase of PDA.

1. Introduction

Polydiacetylenes (PDA) are a class of robust, linear conjugated polymers with alternating triple and double bonds in yne-ene motif. Amphiphilic long-chain diacetylene monomers, compressed at the air-water interface and then UV polymerized form an ultra-thin, stable trilayer structured Langmuir film (LF).[1-3] PDA LF formed on water has unique strand morphology parallel to the polymer direction as a result of its rigid and unbranched linear structure, which provides it with mechanical and chemical stability. This, along with the unique electro-optical properties of polydiacetylenes,[4-6] make them attractive materials for a variety of technological applications such as chemical and biological sensors,[2] resist for lithography,[7,8] effective

template for oriented nucleation of inorganic crystals such as calcite[9, 10] and semiconducting nanocrystals.[11-14]

Polydiacetylenes exist in two principle chromatic phases: a metastable blue phase is obtained directly following the topochemical photopolymerization of diacetylene monomers, and a stable red phase that is the result of prolonged UV irradiation or exposure to other perturbations.[4, 15-19] This visual transformation is the basis for research on PDA potential as chromatic sensors.[2, 4, 9, 19-27] The blue and red phases differ in their short and long-range structural order, which is manifested in scanning force microscopy and absorption spectroscopy.[28] The transition to the stable red phase is accompanied by shortening of the average conjugation length of the polymer [29] and is coincident with the reorganization of the tilted alkyl side chains in the blue phase toward an almost vertical position in the red phase,[1, 30] while the conjugated repeated unit itself remains constant (ca. 4.9Å) for both chromatic phases.[31] The polymerization process is shown schematically in **Figure 1**. While the blue-to-red phase transition of poly-diynoic acids is considered to be irreversible, PDA compounds in which hydrogen bond interactions between headgroups sustain the phase transition exhibited reversible transformations.[32] PDA phase transitions have been shown to be activated biochemically,[2,20,21,34,35] thermally[29] and mechanically.[1, 35, 36] Optical,[19] FTIR,[37] IR,[38] Raman[39] spectrophotometry techniques were previously used in order to monitor PDA phases, and their transitions. An up-to-date summary of PDA chromatic properties was recently published.[40]

Compressed Langmuir films of PCDA (pentacosadiynoic acid) on water typically form trilayer structures parallel to the water surface. The layers are stacked tail-to-tail with hydrophobic van der Waals (VdW) interactions and head-to-head via hydrogen bonds, in an overall amphiphilic vertical structure.

The chiral properties of PDA films were recently studied by Iwamoto and co-workers. Tricosadiynoic acid films produced either by vacuum evaporation[41,42] or Langmuir technique [43,44] were polarized by circular polarized light (CPL). Films polymerized using left or right CPL were found to have the corresponding chirality measured by circular dichroism.

The crystal structure of PDA LF was previously studied by electron diffraction (ED)[31,45] and grazing incidence x-ray diffraction (GIXD) techniques. [46] Both GIXD and ED provide reciprocal space structural information of the monolayer films. However, GIXD data is collected *in-situ*, at the air-solution interface, and does not involve transfer to solid support that can induce damage

and restructuring. Moreover, GIXD has a sizable "footprint" (~50mm^2), it samples large areas, and therefore more reliable. Another advantage of GIXD over ED is its capacity to detect out-of-plane diffraction, emanating from tilted "planes". ED is obtained from very small areas, and is sensitive only to nearly vertical planes, due to the short e-beam wavelength. The GIXD technique is the only method that allows *in-situ* monitoring of crystallographic structural transitions in Langmuir films at the vapor-liquid interface in the real time. In such experiment, a highly monochromatic incident x-ray beam approaches the liquid surface at grazing angle, shallower than the critical angle for reflection, and propagates the surface as an evanescent wave. The physical principle of GIXD method is described elsewhere [47-49]. *In-situ* GIXD structural studies of PDA LF were carried out on single monolayer PDA LF before and after polymerization [46]. The structure of diacetylene films, spread on a sodium tetraborate buffer (pH 7.5), were correlated with its elastic properties. A contraction of the 2D molecular network during polymerization was reported and the nature of the polymerization process was suggested. In this study in-plane diffraction data was collected, but its vertical distribution, pertaining to the planes' tilt was not considered.

Day and Lando [45] studied spontaneously formed PDA monolayer films comprised of 29 carbon-containing diacetylene monomers (nonacosadiynoic acid), and polymerized on Li containing aqueous solution. The PDA samples were transferred horizontally twice onto copper TEM grids, thus forming a misregistered bilayer. They reported a centered rectangular unit cell with a=4.9Å, b=8.11Å cell parameters. In another ED study, tricosadiynoic acid monomers were compressed on subphase containing 0.4mM $CdCl_2$. 19 layers were LB transferred onto TEM grid and UV polymerized. Different centered 2D unit cells for the blue and red PDA structures were reported and were correlated with the optical properties of the films by Kuriyama *et* al.[31]

Common to these works is that the PDA films were stabilized by different salt and buffer solutions containing cadmium, lithium or sodium ions. We have observed that the presence of Zn^{2+} or Cd^{2+} in the subphase considerably affects the structure of PDA (to be published). Hence, earlier reports on PDA films that were produced in the presence of cations in the subphase are not directly comparable to the structures we report here. LF transferred onto solid substrate such as carbon coated TEM grids, glass or mica (for AFM) suffer from some artifactual deviation from its original conformation on the liquid surface.

Here we report on the 2D crystallographic structures of the monomer and two polymer phases of PDA formed on water subphase. The transitions of PDA LF from the unpolymerized

(monomer) state, via the metastable (blue phase) to a final stable state (red phase) were followed in detail, providing information on the sequence of events which occur in these radiation induced structural transformations. The PDA LFs were investigated either directly at the air/water interface using synchrotron GIXD, or after transfer onto amorphous silica-coated TEM grids. The unique structure of the polymerized film was interpreted as two overlaid lipid layers with common lattice points.

2. Results

2.1 GIXD investigation

Langmuir films were prepared on a Langmuir trough mounted on a 6-circle diffractometer at the ESRF beamline 10B.[50,51] Following compression and short UV polymerization, the temperature-controlled trough was translated synchronously with the exposure of newly exposed, "fresh" film segment with each measurement step. Reciprocal space maps of diffracted intensity from PDA LF are presented on orthogonal q_z and q_{xy} diffraction vectors axes. Diffraction from films exposed to progressively higher radiation dose are presented in **Figure 2** (**a** – the lowest dose; **h** and **i** – highest radiation dose).

Figure 2a shows a GIXD map of unpolymerized PCDA film exposed to minimal synchrotron radiation and with no UV irradiation. The crystalline phase represented in **Figure 2a** corresponds closely to the ideal "monomer phase", and has no visible color. Due to the film sensitivity to shortwave radiation, some polymerization could not been avoided. This apparent effect is discussed at section 2.1.3.

The changes in reciprocal space maps from **Figure 2a** to **Figure 2d** represent the gradual progression of topotactic polymerization of PDA LF from the 2D crystalline monomer film to polymerized PDA in the “blue” phase. In order to slow down the polymerization reaction rate the reciprocal maps depicted in **Figure 2a - 2e** were carried out at 5ºC in order to slow the transition rate. **Figures 2d - 2f** depict three structural variations of the “blue” phase obtained along with the gradual appearance of the “red” phase. At this stage the film has a bluish color. The complete “blue” to “red” transition is depicted in **Figures 2e - 2h.** Scans **2e - 2g** allow the monitoring of blue-red coexistence stages. Finally, **Figures 2h, 2i** depict the fully transformed PDA film into the red phase.

Observed and calculated q values of the reflections are presented in **Table 1**. The calculated values are based on unit cell models generated using CaRine® crystallographic software. Also included in **Table 1** are the calculated reflection positions according to the crystallographic model shown in **Figure 3** (columns marked "model"). These peak locations are marked in **Figure 2** using squares (monomer, **Figure 2a)**, triangles (blue phase, **Figure 2d)** and circles (red phase, **Figure 2i)**.

The real space structure schemes of the different PDA film phases formed on water surface are presented in **Figure 3**. According to our underlying structural hypothesis, the film structures are interpreted as consisting of two sub-layers, the methyl-terminated and the carboxyl-terminated alkyl chains on different sides of the diacetylene moiety or polymer backbone (**Figure 1**). It is plausible that these sub-layers have different packing densities and tilt angles due to the different chemical interactions with the subphase, air and mutually at the interlayer hydrophilic and hydrophobic interfaces in the stacked trilayer structure. In **Figure 2**, reflections from the carboxyl-terminated sub-layer were denoted as "1" and from the methyl-terminated sub-layer as "2". M, B and R denote monomer, blue phase and red phase.

For the sake of uniform presentation we use centered rectangular cell notations for all structures.

2.1.1 Monomer phase

While the compressed monomer films are organized in hexagonal order, we present their structure as a centered rectangular cell (a=5.27Å, b=9.13Å, γ=90º) for consistency with the structures of the polymerized phases. The area per molecule is 24.05Å^2. **Figure 2a** depicts the diffraction map obtained from the monomer phase. Two reflections are observed: the hydrophilic chains are not tilted and give rise to a single degenerate $(02,11,\bar{1}1)_{M1}$ broad reflection. In contrast, the hydrophobic chains are tilted by 43° from the normal towards the nearest neighbor (NN), thus breaking the hexagonal symmetry of the "hydrophilic" layer and giving rise to a single, high q_z reflection. According to our structural model, straight chains tilted towards their NN are expected to give the $(02,\bar{1}1)_{M2}$ reflection at q_{xy}=1.37Å^{-1}; q_z=0.84Å^{-1}, as indicated in **Figure 2a**. The observed **arced** reflection, centered at q_{xy}=1.19; q_z= 1.1 has the same q_{tot} value as the calculated $(02)_{M2}$ reflection position. We suggest that the methyl terminated alkyl chains ("2"), fixed at their lattice positions are leaning uniformly towards the [11] direction. The deviation from the

calculated reflection is attributed to chain arcing of the methyl terminated chains, due to the **larger** in-plane spacing originating from the stacked diacetylene moieties (**Figure 5**). The reconstructed 2D scheme of the real space PCDA monomer structure is presented in **Figure 3A**.

2.1.2 Blue phase of PDA

The reciprocal map depicted in **Figure 2d** was used to solve the blue phase structure. Five reflections are observed; three with q_z<0.5 $Å^{-1}$ corresponding to small inclination of the diffracting planes and two highly inclined reflections with q_z>0.8 $Å^{-1}$. Accordingly, the low q_z reflections are attributed to the hydrophilic sub-layer (B1) and the high q_z to the highly tilted hydrophobic sub-layer, B2 (**Table 1**). Using the small inclination reflections, the resulting structure presented in **Figure 3B** by small triangles refers to the PDA carboxyl terminated sub-layer. Similarly, the structure of the highly tilted sub-layer B2 was solved, considering the high q_z reflections, shown in **Figure 3B** by large triangles that refer to highly inclined methyl terminated segments. Note that the "high" and "low" reflections share the same projections onto the q_{xy} axis and x-y plane in **Figures 2d** and **3b**, respectively, indicating a shared underlying in-plane structure. The resulting 2D unit cell of the blue phase is centered oblique with cell parameters (a=4.9Å, b=9.73Å, γ=85°) with in-plane molecular density of 23.73$Å^2$/molecule (alternative presentation: a primitive cell of a=4.9Å, b=5.65Å, γ=59°). Tilt angle of the carboxyl terminated sub-layer from the normal is ca. 18º and that of the methyl terminated is ca. 39º. Based on the lack of q_z component for both $(11)_{B1}$ and $(11)_{B2}$ reflections, we conclude that alkyl chains on both layers are tilted towards the [11] direction, yet in different tilt angles. The direction of the polymer backbone was assigned to be along the a-axis based on its similarity to the distance for the yne-ene conjugation periodicity of a=4.9Å, previously reported by Kuriyama *et* al. [31]

2.1.3 Transition from the monomer to blue phase

The structural changes induced by the topotactic polymerization process from the monomer to the blue phase (M→B) results in breaking of the hexagonal symmetry that characterizes the monomer phase. This reduction in symmetry causes the degenerate $(02, 11, \bar{1}1)_{M1}$ peak to split gradually into separate $(02)_{B1}$, $(11)_{B1}$ and $(1\bar{1})_{B1}$ peaks **(Figures. 2a - 2d**). The structural transformation associated with the formation of the polyconjugated system evidently involves in-plane shear motion of the molecules along the $[11]_{M.B}$ direction. This shear "plane" is dictated by

the tilt direction of the methyl terminated alkyl chains in B2 sub-layer. The transformation of the monomer to the blue phase depicted schematically in **Figures 3A – 3B** results in an oblique cell. We note that in the blue phase, the (11) reflection always persists, suggesting that this plane is the main structural feature of this phase, **Figures 2d - 2f.**

The $(02)_{B1}$ reflection (q_{xy}=1.3Å^{-1}, q_z=0.4Å^{-1}) is diffracted from planes that are parallel to the conjugated polymer backbone. The third reflection from the B1 sub-layer, $(1\bar{1})_{B1}$ reflection, was obtained at q_{xy}=1.49Å^{-1}, q_z=0.45Å^{-1}.

In the course of the gradual restructuring associated with the polymerization of the monomer into the blue phase, we observe two faint reflections that fit neither the monomer, nor the 'blue' structure, **Figures 2a - 2c**. These reflections, located at q_{xy}=1.52Å^{-1}, q_z=0.0Å^{-1} and q_{xy}=1.52Å^{-1}, q_z=0.65Å^{-1} are located on the same q_{tot} arcs as the $(1\bar{1})_{B1}$ and $(1\bar{1})_{B2}$, respectively. **This suggests a two stage mechanism for the structural transition: shear motion of the [11] molecular planes into new lattice positions that allow polymerization, followed by a change in chain tilt angle.** This sequence of events may form a new, highly transient intermediate state that has the same in-plane symmetry as the 'blue' phase, but with upright carboxyl terminated alkyl sub-layer. This transient structural state may well be associated with a phase that has been previously observed and characterized spectrally with main absorption peak around λ=680nm in PDA multilayers.[52]

2.1.4. Blue phase structural variants

At low radiation dose, the $(1\bar{1})_{B2}$ reflection appears as a broad spot centered at q_{xy}=1.49Å^{-1}, q_z=0.95Å^{-1} (**Figure 2d**). Upon increased irradiation, this reflection transforms into a well defined vertical triplet at the same in-plane (q_{xy}) peak position (**Figure 2f**). The Bragg rod triplet structure corresponds to ca. 30Å, in good agreement to single PDA layer height. Similar transition into triplet peak shape with increasing radiation dose is observed also for $(11)_B$.

While strong $(11)_B$ reflection is observed in all the q_{xy}-q_z maps (**Figures 2d-2f**), the other reflections vary in their relative intensities. The $(02)_{B1}$, reflection, observed at q_{xy}=1.29Å^{-1} as a weak reflection in **Figure 2d**, very intense in **Figure 2e** and almost disappearing in **Figure 2f**. These variations indicate that different planes can be highly crystalline, while others lose their registry in the same "blue" phase structure. **Figure 2f,** for example, can represent an intermediate stage in the transition from the blue to the red phase. In the red phase, the distance between adjacent polymer chains is smaller (**Figure 3c**). It is therefore plausible that during the "blue to

red" transition, gradual loss of the crystalline order of the PDA inter-backbone distance takes place, which is manifested in loss of the $(02)_{B1}$ reflection.

Consequently with this process, the $(02)_{B2}$ reflection transformed from the arced reflection described earlier and became better localized, closer to its predicted location. This intermediate state between the "blue" and "red" phases is also accompanied by the appearance of high order $(11)_{B1,B2}$ reflection at $q_{xy}=1.38\text{Å}^{-1}$, $q_z=0.53\text{Å}^{-1}$, which corresponds to the vertical periodicity of ca. 12Å that approximately equals to half of the length of a molecule.

In contrast, the "blue" phase structure indicated in **Figure 2e** is characterized by a well developed $(02)_{B1}$ and $(11)_{B1}$ and faint $(1\bar{1})_{B1}$ reflections. In this variant the arced diffraction from the B2 sub-layer is confined to a narrow q_{tot} spread. These observations suggest that the rows of tilted alkyl chains along the [11] direction are well aligned with respect to their NN both in the "tilt" and in the conjugation directions, but not in the diagonal direction.

The loose packing of the "blue" PDA structure is manifested in its large unit cell area of 23.75Å^2/molecule and provides it with some organizational flexibility. This is revealed by neater order at some directions while increasing the disorder on others. The selection of the ordered vs. disordered directions can vary. The highly tilted layer of leaning alkyl chains, giving rise to the reflection at $q_{xy}=1.3\text{Å}^{-1}$, $q_z=1.02\text{Å}^{-1}$ coordinates is another outcome of the expanded structure that characterizes the PDA blue phase.

2.1.5 Red phase of PDA

Prolonged exposure to UV or x-ray radiation fully transforms the "blue" PDA film into the "red" phase. The diffraction from the red phase is comprised of two low q_z reflection clusters, indicating nearly vertical alkyl chains. As in the case of the monomer and blue phase structures, the red phase is also divided into two sublayers, R1 and R2. The GIXD reciprocal space map of PDA LF in red phase is shown in **Figures 2h** and **2i** and the coordinates and assignments for each reflection are given in **Table 1**.

According to the structure of the red phase, the $(1\bar{1})$ reflection ($q_{xy}=1.59\text{Å}^{-1}$, $q_z=0.1\text{Å}^{-1}$) is common for both sub-layers. The lower, carboxylate terminated sublayer R1 alkyl chains are tilted along **a** direction. The $(02)_{R1}$ reflection is at $q_z=0$, hence untilted at the direction perpendicular to the polymer direction, whereas $(11)_{R1}$ is tilted ($q_{xy}=1.45\text{Å}^{-1}$, $q_z=0.15\text{Å}^{-1}$). The R2 chains are tilted towards its NN along [11] direction. It follows that the overall chain tilt in the R1 layer is 3.5°

towards its neighbor on the same polymer chain in the [10] direction, and the R2 chains are tilted by 5° towards the neighbor polymer backbone in the [11] direction. Low-intensity peaks associated with the red phase consists a "high order" reflections of $(02)_{R2}$ (q_{xy}=1.614Å^{-1}, q_z=0.588Å^{-1}) and of $(11)_{R2}$ (q_{xy}=1.45Å^{-1}, q_z=0.76Å^{-1}) reflections, due to the tri-layered structure of PDA LF and indicate a vertical periodicity of ca. 11Å, roughly half the PCDA molecular length. The 2D crystallographic model of PDA LF in red phase is shown in **Fig. 3C**. Here, as for blue phase, the cell parameters were obtained by the modeling procedure and the a-axis was chosen parallel to the conjugated direction of polymer (a=4.9Å). The resulting 2D crystalline model is presented as a centered quasi-rectangular cell (a=4.9Å, b=7.87Å, γ=84°), with in-plane molecular density of 19.18 Å^2/molecule.

Hence, the blue-to-red transition (B→R) involves a decrease in spacing between the polymer backbones, accompanied with simultaneous upright movement to a near-vertical positioning of both alkyl residues.

2.2 TEM investigation

Unpolymerized and polymerized films were examined by TEM. Relating direct imaging to the reciprocal space diffraction from the same sample region allowed for direct assignment of particular reflections to the real-space image, with reference to the prominent linear strand morphology of PDA. PDA Langmuir films were deposited on amorphous carbon or silica coated copper grids. In order to prevent serious radiation damage, the sample stage was kept at cryogenic temperature (T= -180°C) during the TEM investigations and minimum radiation exposure procedures were practiced. Despite these precautions some beam damage was observed. In order to increase the diffracted signal, selected area diffraction (SAD) was collected with the largest aperture, ca. 0.6μm in diameter. As the typical domain size of PDA films is several μm, this aperture size typically included a single 2D crystal.

TEM images, corresponding SAD patterns and 2D structural schemes derived from GIXD of PDA LF produced on water subphase in monomer and red phases are presented in **Figure 4** and the ED data is summarized in **Table 3.** Miller indices of the obtained reflections are given in "hk" columns; d_{EM} refers to the interplanar distances measured from the diffraction pattern, while d_x is a value calculated from the crystallographic model, based on the x-ray measurements. Usually, the measurement uncertainty of the d_{EM} data is 0.1Å. The measured and calculated angles between the

(11) and ($1\bar{1}$) planes are given by φ_{EM} and φ_X, respectively, allowing to compare the PDA structures obtained from TEM and GIXD.

We note that ED from blue phase could not be acquired, either because it rapidly transforms to the red phase, and/or because as indicated by GIXD, it is not in Bragg condition since all its parts are inclined. In ED, diffraction is obtained exclusively from layers that are nearly normal to the sample plane. According to the GIXD results (**Figure 3**), only the unpolymerized compressed monolayer and the red phase films consist of vertical alkyl chains. The pronounced morphological anisotropy of the PDA images**,** assigned to the PDA conjugated direction **(Figure 4b)** or to its precursor direction in the monomer phase, **(Figure 4a),** were aligned with the 2D crystallographic schemes of the respective phases (**Figures 4e, 4f**). The linear strand morphology, evident in F**igure 4a**, may be an outcome of the high vacuum in the TEM chamber, or due to the some polymerization due to e-radiation. The a-axis direction in the ED pattern of the monomer is ca. 9˚ off from the linear strand direction in the corresponding TEM image (**Figure 4a**). This offset agrees well with our GIXD deduced 2D cells, when the monomer and "blue" cells are aligned with the [11] direction. Hence it provides a quantitative support for the amount of chain slide that is associated with PDA polymerization.

The interplanar distances and angles for monomer phase agree with the 2D hexagonal structure (a=5.27Å, b=9.13Å, γ=90º) of from the vertically oriented alkyl chains, of which calculated values are presented in **Table 3** and depicted graphically in **Figure 3A**. The interplanar distances and angles for the red phase refer to the structure shown in **Figure 3C.** and are in good agreement with the GIXD deduced structure and support the assignment of the a-axis as the polymer backbone direction.

3. Discussion

In this work, we report a combined *in-situ* GIXD and *ex-situ* TEM crystallographic investigation of PDA LFs deposited on a pure water subphase. The techniques corroborate each other and together provide a detailed, coherent picture of the PDA LF. A salient outcome of this study is that the various structural phases and their intermediate states diffract as two different monolayer structures with the same in-plane lattice parameters, yet with different tilt projection and angles. This observation is interpreted as originating from two sub-monolayer structures of the carboxyl and methyl terminated alkyl chains, tethered on the two sides (up/down) of the

(poly)diacetylene moiety. In the monomer and the blue phases, one sub-layer is highly tilted. Based on its intense diffraction, the longer, methyl terminated alkyl chain was assigned to the highly tilted sub-layer. It was found that this extreme tilt of more than 40° from the vertical position plays a crucial role in the structural transformations between the phases. The monomer phase structure is made of a sub-layer of untilted chains in hexagonal arrangement and a second, highly tilted sub-layer. Structural rearrangement during polymerization involves sliding of the monomers along the direction of the tilted chains on the (11) plane. The transition from hexagonal to oblique cell necessarily produces chiral surface arrangement. The Iwamoto group has reported that indeed PDA films are chiral surfaces.[41-44] This work provides a detailed structural mechanism in support of that observation.

The minimal radiation dose procedure employed in the GIXD experiments provided detailed diffraction maps from the unpolymerized film, through several intermediate stages, to the "blue" and subsequently to the "red" phase. The details of the intermediate stages provide valuable insights on the sequence of the transitions between the established solved structures of the monomer, blue and red phases presented in **Figure 3**.

Previous reports on the structure of PDA Langmuir films were based on either electron diffraction [34, 45] or GIXD [46]. It is noteworthy that electrons diffract only from planes that are nearly parallel to the electron beam, hence tilted planes are not detected. In this work ED was used to support the GIXD analyses and to directly assign the identified crystallographic planes with respect to the PDA linear morphological features.

The phase transition process in PDA is continuous from the monomer to the blue and red phases and follows first order kinetics[19,52]. According to our kinetic model, the three phases coexist during the process, as is also observed here (**Figures 2e - 2g**). Yet, it appears that the blue and red phases are structurally distinct and their transformation is discrete, without intermediate states. In contrast, due to their structural similarity, the transformation between the monomer and the blue phase is continuous and involve slight positional shifts of lattice points. As a result, we observe several events that take place during the polymerization and their sequence can be inferred from the GIXD maps (**Figure 2**). Briefly, rows of molecules that are initially in hexagonal positions slide along the direction of their highly tilted alkyl chains towards their neighbors until the required distance for PDA photopolymerization, a=4.9Å, is reached. As a result, the quasi-hexagonal symmetry is reduced to an oblique cell. It follows that the single interplanar spacing,

characteristic of hexagonal structure, gradually splits into two well-defined spacings (**Figures 2a - 2c**). Both the monomer and the blue PDA phases are relatively "expanded" structures with 2 molecules occupying a cell of approximately 50Å^2. This low packing arrangement causes the alkyl chains to tilt abruptly at ~40˚. Moreover, the diffraction obtained from these tilted chains does not fit any indexed interplanar distance of the monomer or the blue phases. It is therefore interpreted as chains that are arced in register from its tether at their lattice point. Hence, the center of mass of their diffraction intensity is shifted. Upon polymerization and the slight compression in cell size, this arced reflection gradually becomes better defined and closer to its calculated position (**Figures 2a - 2g**).

Once the polymer backbone is formed, the fixed conjugated yne-ene repeat unit length of 4.9Å is the main structural constrain. The alkyl chain tilt and other interplanar distances are adjusted accordingly. This could be the origin of metastability of the blue phase. In that way, during B→R transition PDA LF undergoes two processes: 1. shrinkage to a denser molecular arrangement (from area per molecule of 23.73 Å^2 in blue phase to 19.18 Å^2 in red phase) and 2. alkyl chains straightening from the highly tilted position in blue phase to almost vertical in red phase.

The blue to red transformation is driven by the formation of a smaller and more condensed unit cell. The cell shrinkage is caused by reducing the distance between adjacent polymer chains from 4.83Å in the blue to 3.9Å in the red phase, a 20% reduction (**Table 1**). That in turn drives the alkyl chains into a more upright position and as a result to its stable phase. This was also observed by AFM [30]. It is also the reason for the prominent linear "strand" morphology of PDA: the observed lines are actually (02) cleavage planes along the polymer direction, expanded by the reducing inter-backbone distance in the red phase.

4. Experimental Section

4.1 Langmuir film preparation

The experiments were performed either in-house on a standard Nima trough or at beamline ID 10B at ESRF on a custom made Langmuir trough equipped with a single barrier. 50µl of 2mM PCDA chloroform solution was applied with a syringe to the water-air interface. Compression was performed after waiting 15 min for solvent evaporation. The compression rate was 10mm^2 min^{-1}. Compression was usually stopped at a surface pressure of 25mN/m, and the transition from the

monolayer to the trilayer structure was verified to be completed by monitoring the resulting π-A curves.[11] For GIXD investigations the total radiation dose applied to the sample was comprised of two different sources: UV (254 nm) irradiation using a UV lamp (Pen-ray, 4 Watts, UVP), which was mounted within the trough enclosure at a distance of ca. 5cm, and the synchrotron beam. In order to reduce the effect of the latter, the low-dose exposure method was used).

4.2 GIXD characterization

GIXD measurements were carried out at ID 10B beamline at ESRF *in-situ* immediately following film preparation. The Langmuir trough was covered with a sealed enclosure equipped with x-ray transparent Kapton foil windows. In order to minimize damage due to beam-induced free radical formation and excessive x-ray absorption, the chamber was continuously purged with helium so that GIXD measurements were performed with a molecular oxygen concentration <0.3%. High brilliance 8keV synchrotron beam was directed to the interface at 80 percent of the critical angle of total reflection on the water surface, allowing for grazing incidence diffraction from the organic layer. A gas-filled position sensitive detector (PSD) was used to collect the GIXD signal. The experimental setup was recently described by Breiby *et* al. and Smiglies *et* al. [50, 51].

4.3 TEM characterization

For *ex-situ* TEM characterization of PDA films a Tecnai 12 TWIN TEM operating at 80keV was used. Films were lifted from the air-water interface onto holey amorphous silica-coated TEM grids (Cu, 400 mesh, SPI cat. # 02450-AB). Radiation damage of the sample was reduced by using a liquid nitrogen cooled stage. In spite of this, PDA LFs were unstable under the electron beam and tended to burn out after a couple of seconds in diffraction mode.

4.4 Crystalline modeling

The crystalline model of molecular arrangement was fitted for each structural condition of PDA LF. The crystallographic structures were assigned according to the PDA chromatic phases and confirmed using optical spectroscopy[52]: The pre-polymerized phase was determined as monomer phase, the minimal radiation dose condition was assigned to the blue phase, and the final stage of PDA LF obtained after high radiation dose was determined as red phase. The intermediate

structures provided information on the dynamic processes in the PDA LF during the phase transition. After peak assignment, the interplanar distances and their tilt angles according to the horizon were summarized in **Table 1**. Observed reflections were assigned to two sub-structures for the M, B and R phases: carboxyl-terminated (M1, B1, R1) and methyl-terminated (M2, B2, R2) alkyl chains. Both sub-layers have the same 2D in-plane lattice. The peak indexing was done using the CarIne® program using six independent variables (**a, b, c, α, β, γ**). 2D cell parameters (**a, b, γ**) were extracted from the reciprocal space maps by noting the Bragg peak projection on the q_{xy} axis (note that for both sub-structures the peak projections with the similar indices are the same). The parameter **c** refers to the height of the unit cell and was taken as a distance between the next neighboring methyl groups in aliphatic hydrocarbon chain (c=2.53Å). The combination of remaining parameters (**α** & **β**) provides to the tilt value from normal (τ), and azimuthal projection direction of the alkyl chains with respect to the horizontal plane ($sin^2\tau=(cos^2\alpha+cos^2 b-2cos\alpha cos\beta cos\gamma)$)**.** These parameters were fitted in order to match the reflections calculated from the model with the experimental GIXD data.

5. Acknowledgments

Enlightening discussions with Prof. Leslie Leiserowitz from the Weizmann Institute of Science are gratefully acknowledged. We thank Dr. Vladimir Ezersky from BGU for very useful discussions, Dr. Yael Levi-Kalisman for assistance with cryo-TEM and Dr. Dmitry Mogilyanski from BGU for scientific and practical help in modeling the TEM and GIXD results.

This work was supported by the German-Israeli Foundation for Scientific Research and Development (grant G-791-133.10/2003).

We acknowledge the European Synchrotron Radiation Facility for provision of synchrotron radiation facilities at ID10B beamline.

5. References

[1] R. W. Carpick, D. Y. Sasaki, M. S. Marcus, M. A. Eriksson, A. R. Burns, *J. Phys.: Condens. Matter* **2004**, *16*, R679

[2] D. Charych, J. D. Nagy, W. Spevak, M. Bednarski, *Science* **1993**, *261*, 585

[3] Z. Huilin, L. Weixing, Y. Shufang, H. Pingsheng, *Langmuir* **2000**, *16*, 2797

[4] W. Wensel, G. H. Atkinson, *J. Am. Chem. Soc.* **1989**, *111*, 6123

[5] J. M. Pigos, Z. Zhu, J. L. Musfeldt, *Chem. Mater.* **1999**, *11*, 3275

[6] T. Ravindran, W. H. Kim, A. K. Jain, J. Kumar, S. K. Tripathy, *J. Phys.: Condens Matter.* **1995**, *7*, 1315

[7] N. G. Semaltianos, H. Araujo, E. G. Wilson, *Surf. Sci.* **2000**, *460*, 182

[8] M. D. Mowery, A. C. Smith, C. E. Evans, *Langmuir* **2000**, *16*, 5998

[9] A. Berman, D. J. Ahn, A. Lio, M. Salmeron, A. Reichert, D. Charych, *Science* **1995**, *269*, 515

[10] K. Sato, Y. Kumagai, T. Kogure, K. Watari, J. Tanaka, *J. Ceram. Soc. Jpn.* **2006**, *114, 9*, 754

[11] A. Berman, D. Charych, *J. Crys. Growth* **1999**, *198/199*, 796

[12] N. Belman, A. Berman, V. Ezersky, Y. Lifshitz, Y. Golan, *Nanotechnology* **2004**, *15*, S316

[13] A. Berman, N. Belman, Y. Golan, *Langmuir* **2003**, *19*, 10962

[14] Y. Lifshitz, O. Konovalov, N. Belman, A. Berman, Y. Golan, *Adv. Funct. Mater.* **2006**, *16*, 2398

[15] J. Kajser, G. Wegner, E. W. Fischer, *Isr. J. of Chem.* **1972**, *10*, 157

[16] B. Tieke, G. Wegner, D. Naegele, H. Ringsdorf, *Angew. Chem. Int. Ed. Engl.* **1976**

[17] Y. Tokura, K. Ishikawa, K. Kanetake, T. Koda, *Phys. Rev. B* **1987**, *36*, 2913

[18] B. J. Orchard, S. K. Tripathy, *Macromol.* **1986**, *19*, 1844

[19] U. G. Hofmann, J. Peltonen, *Langmuir* **2001**, *17*, 1518

[20] Y. Scindia, L. Silbert, R. Volinsky, S. Kolusheva, R. Jelinek, *Langmuir* **2007**, *23*, 4682

[21] S. Kolusheva, T. Shahal, R. Jelinek, *J. Am. Chem. Soc.* **2000**, *122*, 176

[22] J. Xu, X. Ji, K. M. Gattá-Asfura, C. Wang, R. M. Leblanc, *Colloids Surf., A* **2006**, *284 - 285*, 35

[23] J. Pang, L. Yang, B. F. McCaughey, H. Peng, H. S. Ashbaugh, C. J. Brinker, Y. Lu, *J. Phys. Chem. B* **2006**, *110*, 7221

[24] N. Y. Lee, Y. K. Jung, H. G. Park, *J. Biochem. Eng.* **2006**, *29*, 103

[25] Z. Yuan, C.-W. Lee, S.-H. Lee, *Polymer* **2005**, *46*, 3564 – 3566

[26] J.-M. Kim, Y. B. Lee, D. H. Yang, J.-S. Lee, G. S. Lee, D. J. Ahn, *J. Am. Chem. Soc.* **2005**, *127*, 17580

[27] E. Geiger, P. Hug, B. A. Keller, *Macromol. Chem. Phys.* **2002**, *203*, 2422

[28] A. Lio, A. Reichert, D. J. Ahn, J. O. Nagy, M. Salmeron, D. Charych, *Langmuir* **1997**, *13*, 6524

[29] Y. Tomioka, N. Tanaka, S. Imazeki, *J. Chem. Phys* **1989**, *91*, 5694

[30] D. Y. Sasaki, R. W. Carpick, A. R. Burns, *J. Col. Int. Sci.* **2000**, *229*, 490

[31] K. Kuriyama, H. Kikuchi, T. Kajiyama, *Langmuir* **1998**, *14*, 1130

[32] J. M. Kim, J. S. Lee, H. Choi, D. Sohn, D. J. Ahn, *Macromolecules* **2005,** *22*, 9366.

[33] Q. Huo, K. C. Russell, R. M. Leblanc, *Langmuir* **1999**, *15*, 3972

[34] Q. Cheng, R. C. Stevens, *Langmuir* **1998**, *14*, 1974

[35] R. W. Carpick, D. Y. Sasaki, A. R. Burns, *Langmuir* **2000**, *16*, 1270

[36] C. H. Lee, E. H. Oha, J. M. Kim, D. J. Ahn, *Colloids and Surf.* **2008**, *313/*, 500

[37] D. J. Ahn, A. Berman, D. Charych, *J. Phys. Chem.* **1996**, *100*, 12455

[38] A. Saito, Y. Urai, K. Itoh, *Langmuir* **1995**, *12*, 3938

[39] A. Materny, T. Chen, A. Viertheilin, W. Kiefer, *J. Raman Spectrosc.* **2001**, *32*, 425

[40] M. Schott, *J. Phys. Chem. B* **2006**, *110*, 15864

[41] T. Manaka, H. Kon, Y. Ohshima, G. Zou, M. Iwamoto, *Chem. Lett.* **2006**, *35*, 1028

[42] H. Kohn, Y. Oshima, T. Manaka, M. Iwamoto, *Jap. J. of App. Phys.* **2008**, *47*, 1359
[43] G. Zou, H. Kohn, Y. Ohshima, T. Manaka, M. Iwamoto, *Chem. Phys. Lett.* **2007**, *442*, 97
[44] G. Zou, T. Manaka, D. Taguchi, M. Iwamoto, *Colloids Surf. A* **2006**, *284 - 285*, 424
[45] D. Day, J. B. Lando, *Macromol.* **1980**, *13*, 1483
[46] C. Gourier, M. Alba, A. Braslau, J. Daillant, M. Goldmann, C. M. Knobler, F. Rieutord, G. Zalczer, *Langmuir* 2001, *17*, 6496
[47] J. Als-Nielsen, D. Jacquemain, K. Kjaer, F. Leveiller, M. Lahav, L. Leiserowitz, *Phys. Rep.* **1994**, *246*, 251
[48] T. R. Jensen, K. Balashev, T. Bjørnholm, K. Kjaer, *Biochimie* **2001**, *83*, 399
[49] V. Kaganer, H. Möhwald P. Dutta, *Rev. Mod. Phys.* **1999**, *71*, 779
[50] D. W. Breiby, E. J. Samuelsen, O. Konovalov, B. Struth, *Langmuir* **2004**, *20*, 4116
[51] D. M. Smilgies, N. Boudet, B. Struthb, O. Konovalov, *J. Synchrotron Rad.* **2005**, *12*, 329
[52] Y. Lifshitz, O. Shusterman, A. Upcher, Y. Golan, A. Berman, B. Horovitz, *in preparation* **2008**

Figures and Tables

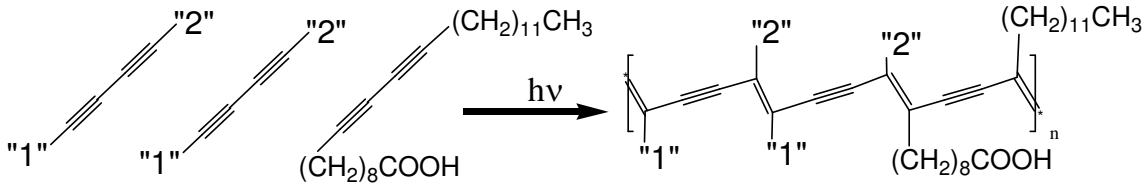

Figure 1: Topotactic polymerization of diacetylene lipid PCDA. The yne-ene conjugated backbone carries a polar and a-polar side chains, denoted "1" and "2", respectively.

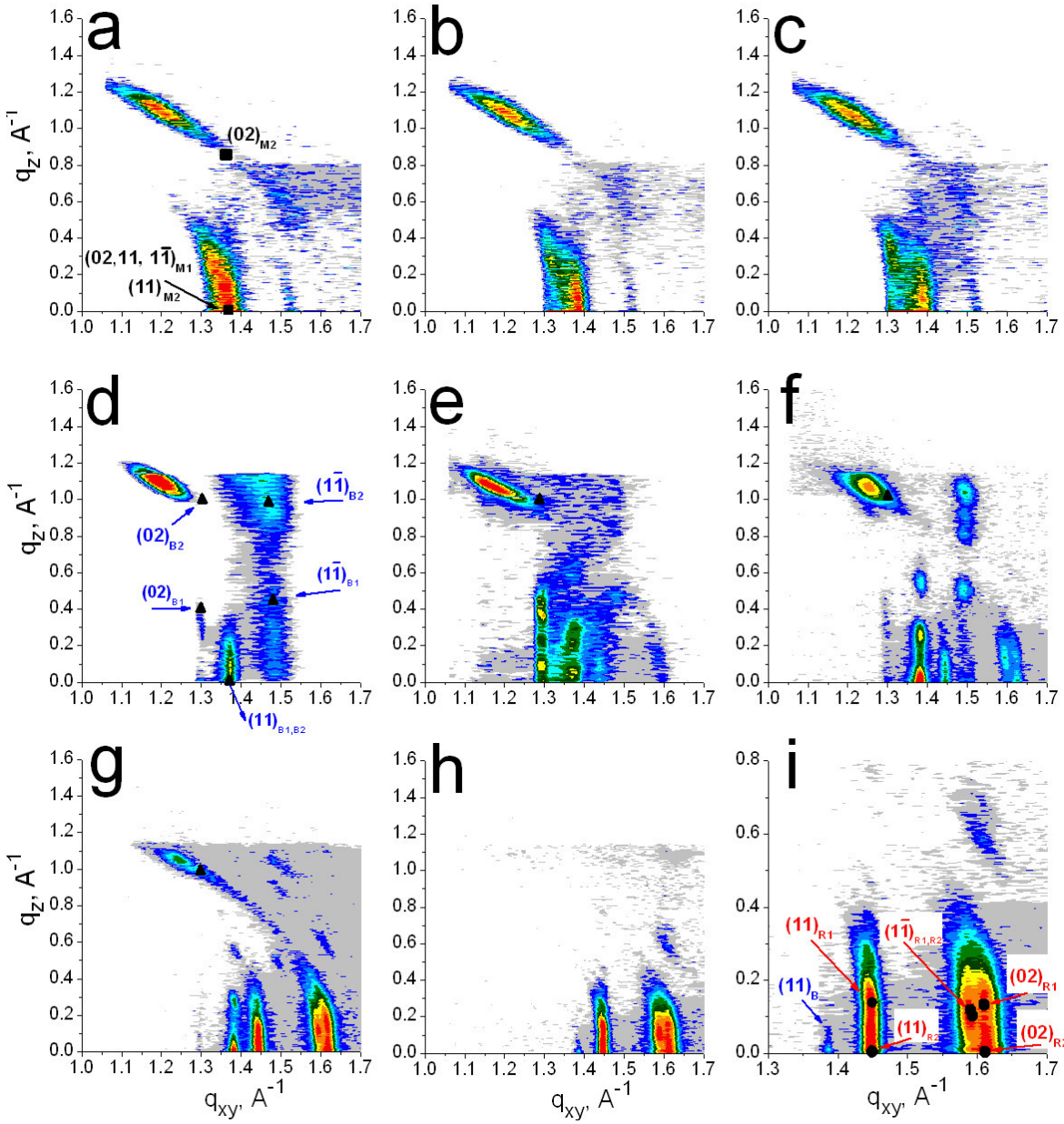

Figure 2: GIXD reciprocal space maps (I=*f*(q_{xy}, q_z)) obtained from PDA LF. Each map (a-h) corresponds to progressively increasing integrated (synchrotron and UV) radiation dose (from **a** – the lowest dose, to **h** – highest radiation dose). Map **i** is the enlarged region of **h**. Scans **a**, **b**, **c** and **g** were taken at 5ºC, and the rest at room temperature. The calculated positions based on the crystallographic model presented in **Table 1** are marked by squares in "**a**" for monomer, triangles in "**d**" for blue phase and circles in "**i**" for red phases. All Miller indices refer to the centered cells for all phases (see **Figure 3**).

Table 1: Summary of the GIXD reflections presented in **Figure 2**. Reflections assignment was based on two layered structures for each PDA phase: M1, B1, R1 - for the hydrophilic and M2, B2, R2 - for the hydrophobic segments according to **Figure 1**. q_{xy} and q_z are the peak coordinates in reciprocal space; $q_{tot} = (q_{xy}^2+q_z^2)^{1/2}$ is the reciprocal interplanar distance, τ is the tilt angle of the diffraction vectors with respect to the normal. The 'Model' columns are the calculated interplanar distances and tilt angles of all reflections according to the crystallographic model of the monomer, blue and red phases structures presented in **Figure 3**. The "Model" q_{xy} and d_{xy} columns represent the interplanar spacings in the 2D unit cell for each phase.

Phase	Miller Indices	Measured reflections				Model			
		q_{xy}, Å^{-1}	q_z, Å^{-1}	q_{tot}, Å^{-1}	τ °	q_{tot}, Å^{-1}	τ °	q_{xy}, Å^{-} $_1$	d_{xy}, Å
M1	02,11,1$\bar{1}$	1.37	0	1.37	0	1.37	0	1.37	4.58
M2	11	1.37	0	1.37	0	1.37	0	1.37	4.58
M2	02,1$\bar{1}$	1.19	1.1	1.62	42.75	1.61	31.7	1.37	4.58
B1	02	1.3	0.4	1.35	17.2	1.36	17.4	1.3	4.83
B1*	11	1.38	0	1.38	0	1.38	0	1.38	4.55
B1	1$\bar{1}$	1.49	0.45	1.55	16.1	1.55	15.3	1.49	4.21
B2*	11	1.38	0	1.38	0	1.38	0	1.38	4.55
B2	02	1.19	1.1	1.62	42.75	1.60	35.9	1.3	4.83
B2	1$\bar{1}$	1.49	0.95	1.76	32.4	1.77	32.3	1.49	4.21
R1	11	1.45	0.15	1.45	5.9	1.46	5.7	1.45	4.33
R1	1$\bar{1}$	1.59	0.1	1.59	3.6	1.59	4.1	1.59	3.96
R1	02	1.61	0	1.61	0	1.61	0.5	1.61	3.9
R2	11	1.45	0	1.45	0	1.45	0	1.45	4.33
R2	1$\bar{1}$	1.59	0.1	1.59	3.6	1.59	4	1.59	3.96
R2	02	1.61	0.15	1.62	5.3	1.61	4	1.61	3.91

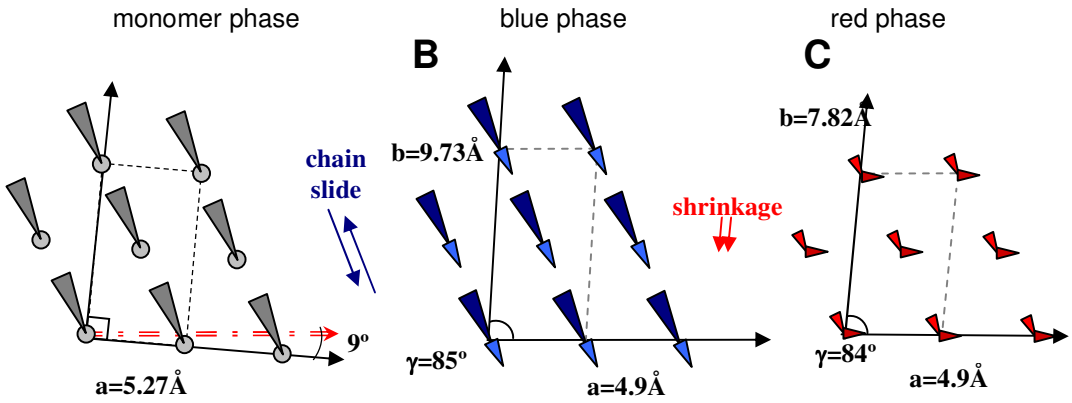

Figure 3: Schematic representation of M→B→R phase transitions of PDA LF on pure water starting from the unpolymerized monomer phase (denoted **A**) via metastable blue phase (**B**), and finally to the stable red phase (**C**). The tilt direction of the alkyl chains tilt is denoted by triangles. The triangle sizes represent to the chain projection on the plane, hence, their tilt. The "**a**" and "**b**" axes correspond to the centered cell for each structure. For blue and red phases the **a** direction is defined along the conjugated direction of the polymer, while for the monomer phase the direction of upcoming polymer is marked by a red arrow. In **A** and **B**, the chain tilt directions are parallel. In **B** and **C**, the **a** crystallographic directions are co-aligned. The structural information for each phase is summarized in **Table 2**.

Table 2: Summary of the structural parameters of all three phases of the PDA LF. The cell parameters and tilt directions correspond to the structures presented in Fig. 3.

	Monomer	Blue phase	Red phase
Cell parameters	a=5.27Å b=9.13 Å γ=90º	a=4.9Å b=9.73 Å γ=85º	a=4.9Å b=7.82 Å γ=84º
Area/molecule	24.05 Å^2	23.74 Å^2	19.18 Å^2
Calculated molecular tilt (from model)	M1=0, M2=43º[11]	B1=18º [11], B2=39º [11]	R1=5º [11], R2=3.5º [10]

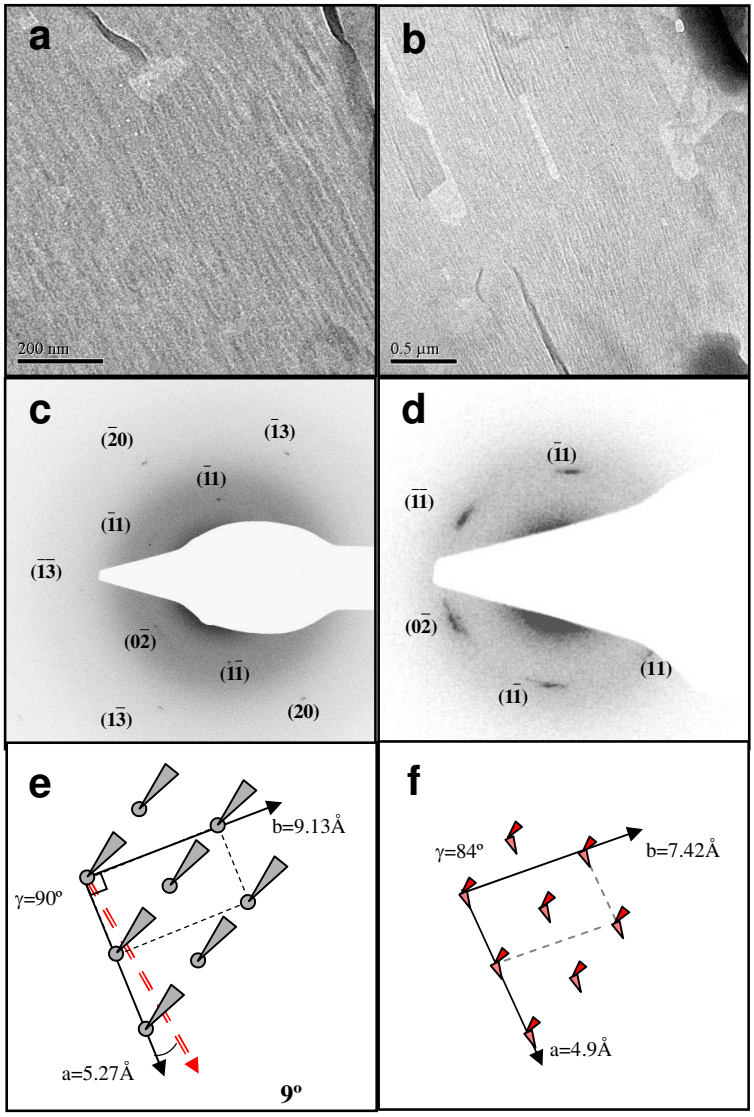

Figure 4: TEM images and ED of PDA LF produced on water subphase in monomer (a, c) and red (b, d) phases. The SAD in images **c** and **d** are taken from the regions in **a** and **b**, respectively. **e** and **f** represent the 2D crystallographic models calculated from the GIXD results (see also **Figures 3A**, **3C**) rotated to fit the micrographs and ED patterns. Dashed arrow in **e** indicate the a axis direction in the subsequent polymer.

Table 3: Summary of ED data presented in **Figure 4**. "hk" columns list the Miller indices d_{EM} are the interplanar distances measured by electron diffraction; d_X are calculated from the crystallographic model, based on the GIXD measurements. The measured and calculated angles between the (11) and $(1\bar{1})$ planes are given by φ_{EM} and φ_X, respectively. Note that the blue phase was not observed in TEM due to its tilted structure and its metastability.

Monomer phase					Red phase				
hk	d_{EM}, Å	d_X, Å	φ_{EM}	φ_X	hk	d_{EM}, Å	d_X, Å	φ_{EM}	φ_X
11	4.53	4.58	60.9º	60º	11	4.25	4.35	63.75º	64.14º
$\bar{1}\bar{1}$	4.53	4.58			$\bar{1}\bar{1}$	4.25	4.35		
02	4.52	4.58			$\bar{1}1$	3.98	3.95		
$\bar{1}1$	4.5	4.58			$1\bar{1}$	3.88	3.91		
$1\bar{3}$	2.61	2.64			02	4.05	3.95		
13	2.6	2.64							
$\bar{1}\bar{3}$	2.6	2.64							
20	2.59	2.64							
$\bar{2}0$	2.59	2.64							

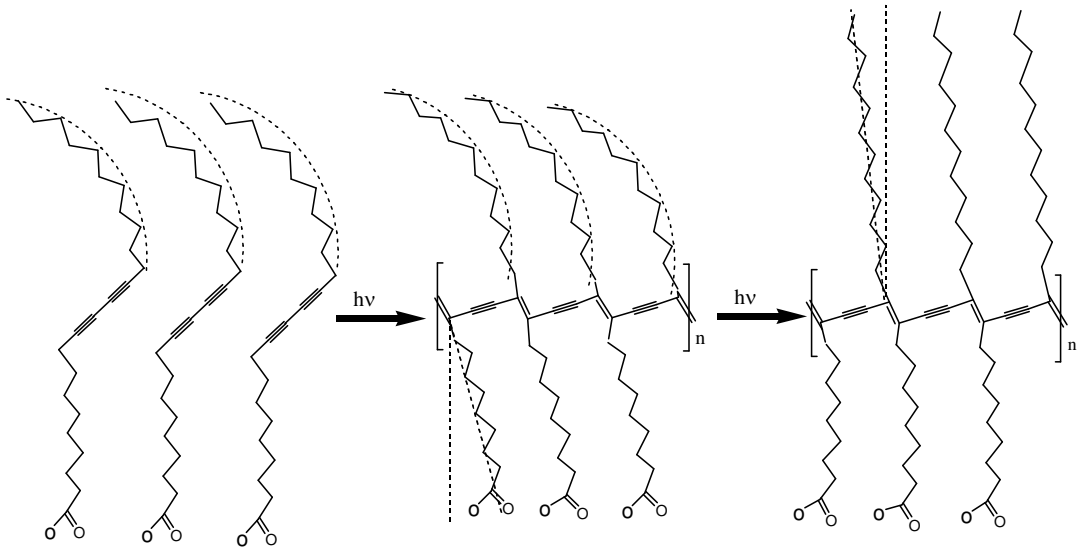

Figure 5: Schematic drawing of PDA phase transition, left: polymerization, referred to here as M→B transition. Right: blue to red phase transition. Depicted in this drawing are some of the conclusions of this work. Note (i) the different conformation of the methyl vs. carboxyl terminated chains (ii) the arced methyl terminated chains in the monomer and "blue" phases. (iii) the different tilt angle of the chains in the monomers vs. the polymerized "blue" phase. This drawing is roughly from the a* direction (perpendicular to the polymer backbone), but the chains tilt has a diagonal component into the drawing plane)